© 2015. Published by The Company of Biologists Ltd | The Journal of Experimental Biology (2015) 218, 1748-1758 doi:10.1242/jeb.120824

RESEARCH ARTICLE

Locomotor corollary activation of trigeminal motoneurons: coupling of discrete motor behaviors

Sara Hänzi[1,2,*], Roberto Banchi[1,2,*], Hans Straka[1,‡] and Boris P. Chagnaud[1,‡,§]

ABSTRACT

During motor behavior, corollary discharges of the underlying motor commands inform sensory-motor systems about impending or ongoing movements. These signals generally limit the impact of self-generated sensory stimuli but also induce motor reactions that stabilize sensory perception. Here, we demonstrate in isolated preparations of *Xenopus laevis* tadpoles that locomotor corollary discharge provokes a retraction of the mechanoreceptive tentacles during fictive swimming. In the absence of sensory feedback, these signals activate a cluster of trigeminal motoneurons that cause a contraction of the tentacle muscle. This corollary discharge encodes duration and strength of locomotor activity, thereby ensuring a reliable coupling between locomotion and tentacle motion. The strict phase coupling between the trigeminal and spinal motor activity, present in many cases, suggests that the respective corollary discharge is causally related to the ongoing locomotor output and derives at least in part from the spinal central pattern generator; however, additional contributions from midbrain and/or hindbrain locomotor centers are likely. The swimming-related retraction might protect the touch-receptive Merkel cells on the tentacle from sensory over-stimulation and damage and/or reduce the hydrodynamic drag. The intrinsic nature of the coupling of tentacle retraction to locomotion is an excellent example of a context-dependent, direct link between otherwise discrete motor behaviors.

KEY WORDS: Corollary discharge, Efference copy, Spinal locomotion, Trigeminal nerve, *Xenopus laevis*

INTRODUCTION

During rhythmic locomotion, a number of otherwise independent movements are influenced by the rhythm of the motor commands. In vertebrates, such coupling is observed for respiration (Bramble and Carrier, 1983), eye movements (Lambert et al., 2012), tail motion (Wada et al., 1993) or phase-locked arm and trunk motor adjustments (Earhart, 2013). While some coupled motor behaviors such as tail motion, e.g. in dogs, improve locomotor performance (Wada et al., 1993), others improve sensory acquisition and processing as observed for retinal image stabilization (Chagnaud et al., 2012a; Lambert et al., 2012). One possibility for coupling otherwise unrelated motor behaviors to locomotion is via corollary discharge that derives from spinal or supraspinal locomotor centers. These signals allow fast and reliable phase locking of the respective motor behavior to the locomotor rhythm (Chagnaud et al., 2012a). Corollary discharges are independent of locomotor style and occur during rhythmic limb-based locomotion in terrestrial vertebrates as well as during body/tail-based swimming in aquatic vertebrates (Chagnaud et al., 2012a). Traditionally, motor corollary discharges have been described as mechanisms to differentiate between environmental and self-generated sensory inputs (Crapse and Sommer, 2008; Cullen, 2004, 2011; von Holst and Mittelstaedt, 1950; Poulet and Hedwig, 2007; Sommer and Wurtz, 2008). In contrast, the impact of motor corollary discharges on motor systems and the indirect effects on the sensory encoding have been less well investigated. Some studies have shown that corollary discharge can cause reflex inhibition during swimming in *Xenopus* embryos (Sillar and Roberts, 1988), suppress withdrawal responses in gastropods during feeding behavior (Davis et al., 1974; Kovac and Davis, 1980) and drive compensatory eye movements during swimming in larval *Xenopus* (Lambert et al., 2012). However, attempts to decipher the mechanisms underlying the effects of corollary discharge on motor behaviors are often constrained by the complexity of the central nervous system and the limb-based locomotion. In contrast, tail-based swimming in amphibians (Wassersug and Hoff, 1985) and fishes represents a simple, stereotyped locomotor pattern with correspondingly simpler spatio-temporal profiles of corollary discharges.

A number of aquatic anamniotes possess various numbers of mobile appendages on the head that contain several types of sensors (see Fox, 1999). One example is the pair of rostrally protruding tentacles in *Xenopus laevis* Daudin tadpoles that are equipped with Merkel cells (Ovalle, 1979). The mechanosensory nature of these cells (Maricich et al., 2009) suggests an important role for touch discrimination and surface structure recognition. Because of the location of the tentacles on the head and the tadpole's undulatory swimming style with prominent horizontal head oscillations, the tactile function of these appendages might be impaired during locomotor behavior. Given the previously reported spinal efference copy-driven compensatory eye motion in *Xenopus* tadpoles during swimming (Combes et al., 2008; Lambert et al., 2012), a protection of the sensor and a potential improvement of propulsive efficacy could be achieved by a similar spinal locomotor corollary discharge that causes a tentacle retraction.

Here, we provide direct evidence that locomotor corollary discharges during rhythmic swimming in *X. laevis* tadpoles initiate a bilateral tentacle retraction. Fluorescent tract tracing, Ca^{2+} imaging, electrophysiological recordings and video analysis of tentacle motor behavior during fictive locomotion in semi-intact *in vitro* preparations outline the underlying trigeminal motoneuronal populations, their firing pattern and their link to ongoing locomotor commands. The observed coupling of tentacle retraction to swimming is an excellent example of intrinsic control of a particular motor behavior that is otherwise unrelated to locomotion.

[1]Department Biology II, Ludwig-Maximilians-University Munich, 82152 Planegg, Germany. [2]Graduate School of Systemic Neurosciences, Ludwig-Maximilians-University Munich, 82152 Planegg, Germany.
*These authors contributed equally to this work
‡These authors contributed equally to this work

§Author for correspondence (b.chagnaud@lmu.de)

Received 16 February 2015; Accepted 30 March 2015

The Journal of Experimental Biology

The Journal of Experimental Biology (2015) 218, 1748-1758 doi:10.1242/jeb.120824

RESULTS

Locomotion-coupled tentacle motion

Xenopus laevis tadpoles are equipped with a bilateral, mobile pair of tentacles (Cannone and Kelly, 1977; Ovalle, 1979) that are attached to the upper jaw at the lateral aspect of the mouth. At rest, these appendages extend rostro-laterally (Fig. 1Ai,B) at an angle of 19±10 deg (mean±s.d., 61 tentacles) relative to the longitudinal body axis. During fictive locomotion, indicated by rhythmic bursts in spinal ventral roots (VRs) in isolated tadpole preparations (Combes et al., 2004; see below for details), video recordings revealed that the tentacles were concurrently retracted (Fig. 1Aii). The maximal retraction angle during swimming was 115±24 deg (61 tentacles, n=41 swimming episodes in N=7 preparations; Fig. 1B). During locomotor activity, the tentacles essentially remained in a lateral position interspersed by variably timed and sized oscillations (Fig. 1C). As the locomotor activity ceased, the tentacles protracted towards the initial resting position (Fig. 1Aiii, Aiv, Ci).

Simultaneous video recordings of the tentacles on both sides (n=20 episodes in N=4 preparations) yielded very similar motion dynamics and trajectories of both tentacles during a given locomotor episode (see red and blue traces in Fig. 1Ci). The close coupling of onset, duration and motion pattern of the left and right tentacle was verified by correlating the respective motion trajectories (Fig. 1Cii). The distribution of the correlation coefficients (median: 0.81; Fig. 1D) was significantly different from zero (P<0.0001; Wilcoxon signed-rank test) indicating that both tentacles move symmetrically. This close match of the bilateral motor activity was exploited in subsequent experiments by combined recordings of the motion pattern of one tentacle and the neuronal commands of the trigeminal motor nerve that innervates the tentacle on the other side. Moreover, the presence of tentacle movements during locomotion in completely isolated and immobile *Xenopus* tadpole preparations and thus in the absence of tail motion-related sensory signals suggests that the motor commands derive from a locomotor corollary discharge that activates the tentacle motor system.

Anatomical organization of the tentacle motor system

Tentacle movements in *Xenopus* tadpoles are produced by a single muscle (m. levator mandibulae pars lateralis) that retracts the tentacle (Nieuwkoop and Faber, 1994); in contrast, protraction of the tentacle occurs in the absence of a respective muscle but likely involves the mechanics of a cartilaginous spring (Ovalle et al., 1998). The tentacle muscle, responsible for the retraction, has a joint proximal origin with the jaw closing muscles (m. levator mandibulae pars intermedius and medialis) but remains otherwise separate (dashed line in Fig. 2B), and attaches distally at the cartilaginous base of the tentacle (Fig. 2A,B). The exclusive control of tentacle movements by the lateral portion of the m. levator mandibulae was demonstrated by a set of differential muscle lesions. A specific transection (three preparations) of the m. levator mandibulae pars lateralis, which left the other two portions of the m. levator mandibulae intact, abolished all tentacle movements. In contrast, a reciprocal surgical intervention (three preparations), that preserved the lateral portion, left tentacle movements unaffected. The sensory-motor innervation of the tentacle and its muscle is formed by the trigeminal ophthalmic (rOP) and mandibular branches (rMA) as illustrated by the pattern of labeled peripheral nerves following application of biocytin to the trigeminal nerve root close to the hindbrain (Fig. 2A). The motor innervation of the tentacle muscle, however, originates exclusively from the smaller branch (tentacle nerve, TN) after ramification of the rMA into two branches at the level of the m. levator mandibulae (red asterisk in Fig. 2B).

Apart from innervating the tentacle muscle, the TN branch also innervates the jaw closing muscle (Fig. 2A,B). This branch exclusively contains motor axons as indicated by the absence of sensory hindbrain projections following tracer application to this particular nerve (left side in Fig. 2C). This differs from the observed pattern after labeling of the second rMA branch (blue arrowhead in Fig. 2B) or the trigeminal nerve root, where

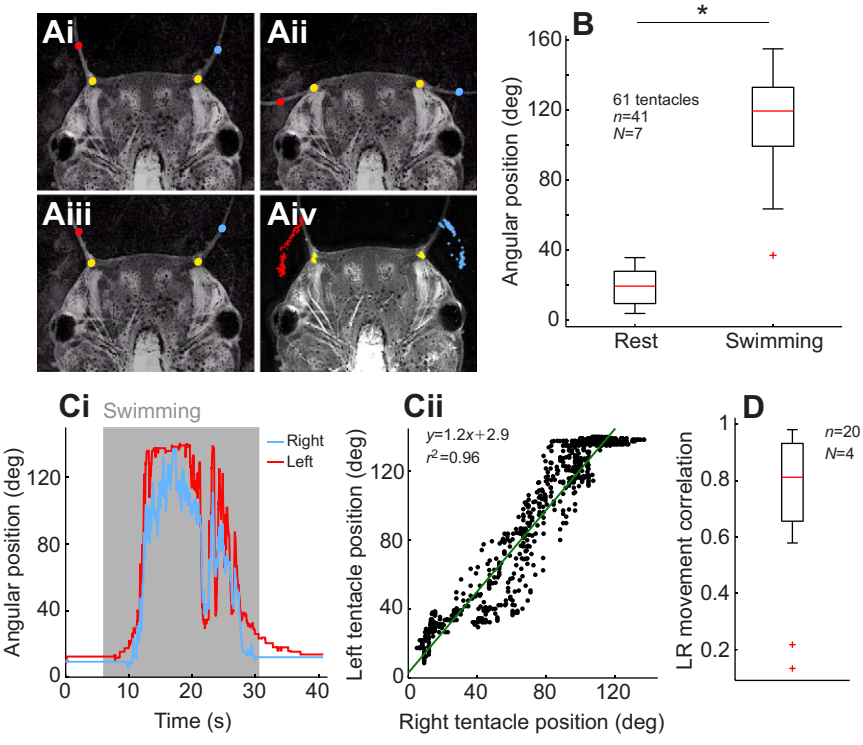

Fig. 1. Bilaterally coordinated tentacle movements during fictive swimming in an isolated *in vitro Xenopus laevis* tadpole preparation. (A) Representative frames from a video recording before (Ai), during (Aii) and after (Aiii) an episode of fictive swimming; positions of the left and right tentacle and their proximal insertions (yellow) are superimposed on an image overlay (Aiv) visualizing the trajectories during the entire locomotor event. (B) Boxplots of angular tentacle positions at rest and at maximal eccentricity (relative to the longitudinal body axis) during fictive swimming (61 tracked tentacles, obtained from n=41 locomotor episodes in N=7 preparations). (Ci) Angular trajectory of the left and right tentacle during an episode of fictive swimming (gray area); (Cii) scatter plot and linear regression correlating the angular positions of the two tentacles during the locomotor episode shown in Ci. (D) Boxplot of correlation coefficients between angular positions of the left and right (LR) tentacles during n=20 swimming episodes in N=4 preparations with a median coefficient of 0.81 (P<0.0001; Wilcoxon signed-rank test).

The Journal of Experimental Biology (2015) 218, 1748-1758 doi:10.1242/jeb.120824

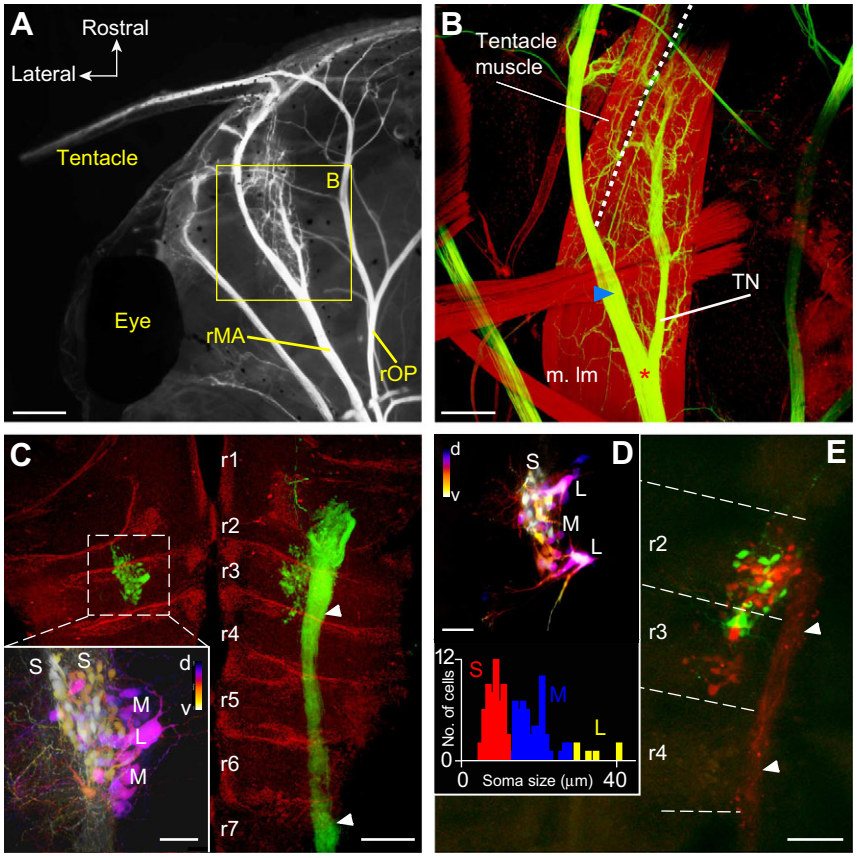

Fig. 2. Anatomical organization of the tentacle motor system. (A) Wide-field fluorescence image, depicting the left tentacle and its biocytin/streptavidin-Cy2-labeled (in white) neuronal innervation by the ophthalmic (rOP) and mandibular branch (rMA) of the trigeminal nerve. (B) Confocal reconstruction of the area outlined in A, illustrating the tentacle muscle – lateral portion (dashed line) of the m. levator mandibulae (m. lm) – and the tentacle nerve (TN) that branches off (red asterisk) from the main rMA (blue arrowhead); confocal scanning at 488 and 633 nm visualized biocytin/streptavidin-Cy2-labeled trigeminal nerve branches (green) and muscle tissue (red). (C–E) Confocal reconstruction of trigeminal motoneurons and afferent projections in the hindbrain (white arrowheads in C, E), labeled with biocytin/streptavidin-Cy2 or Alexa Fluor dextran 488/546 from the TN (left side in C, D; green neurons in E), the trigeminal nerve root (right side in C) or the main rMA (red neurons in E) distal to the TN branching (blue arrowhead in B); rhombomere (r1–7) boundaries (C) were visualized with 633 nm illumination; tentacle motoneurons, color coded according to their position along the *z*-axis (inset in C, D), subdivide into dorso-medially located large (L) and medium-sized (M) elongated cells and ventro-laterally located small, round cells (S); the dorso-ventral extension of the *z*-stack is 74 µm in the inset in C and 128 µm in D. The histogram in the lower part of D displays the distribution of soma diameters across preparations. Color code: d, dorsal; v, ventral. Scale bars are 0.5 mm in A, 0.2 mm in B, C and E, and 50 µm in C inset and D. Arrows in A indicating the rostral and lateral direction apply to all other panels.

additional dense afferent terminations were observed in the dorsal hindbrain throughout r1–r7 (arrowheads on the right side in Fig. 2C,E), indicating the presence of sensory fibers in the respective nerves.

The hindbrain location of motoneurons innervating the tentacle muscle was compared with the entire population of trigeminal motoneurons following application of biocytin to the TN at its entrance into the muscle or to the trigeminal nerve close to the hindbrain (cell groups on the left and right side, respectively, in Fig. 2C). Tracer application to the TN consistently labeled a group of motoneurons in hindbrain segments r2 and r3 (left side in Fig. 2C–E). This bi-segmental location coincides with that of the entire population of trigeminal motoneurons, labeled from the trigeminal nerve root (right side in Fig. 2C). The number of retrogradely labeled tentacle motoneurons was variable and ranged from 9 to 87 neurons in different experiments (median: 27 cells, *N*=10 preparations). These motoneurons only innervated the m. levator mandibulae because labeling of the TN and the second rMA branch (blue arrowhead in Fig. 2B) in different colors (Alexa Fluor dextran 488 and 546; *N*=4 preparations) did not yield double-labeled neurons (see absence of yellow cells in r2 and r3 in Fig. 2E). However, tentacle motoneurons were intermingled with other rMA motoneurons (green and red cells in r2 and r3 in Fig. 2E) within the trigeminal nucleus.

Tentacle motoneurons form a heterogeneous population with respect to soma size and shape (inset in Fig. 2C,D). A histogram of soma diameters (120 cells in *N*=6 preparations) revealed that cell size extends over a large range that suggests the presence of up to three groups of neurons with a tendency for a size-related dorso-ventral separation (see Fig. 2C,D inset for *z*-axis color-coded confocal reconstruction). Neurons were categorized as either small (<12 µm) and mostly round (group 1: S) or medium sized (≥12 and <30 µm) with oval somata (group 2: M) with the consistent exception of one to two very large (≥30 µm) neurons with elongated cell bodies (group 3: L), located at the most dorso-medial aspect of the labeled cell group (L in Fig. 2C,D inset). Medium-sized neurons were located at more medial and dorsal positions relative to the smaller cells (Fig. 2C,D inset). The mean size of the neurons was 8.3±1.9 µm (56 cells) for small neurons, 18.1±3.8 µm (58 cells) for medium neurons and 34.6±4.4 µm (six cells) for large neurons. Accordingly, tentacle motoneurons form a morphologically diverse and dispersed cell group within the trigeminal motor nucleus in r2 and r3 with a size-related dorso-ventral arrangement.

Activity of tentacle motoneurons during locomotion

The morphological diversity of tentacle motoneurons prompted us to test whether all or only a particular subpopulation of motoneurons become active during swimming and cause the observed tentacle retraction. Neuronal activity was measured as Ca^{2+} transients in the entire tentacle motor nucleus or in individual motoneurons, following unilateral or bilateral application of Calcium Green-1 dextran to the peripheral motor target(s) and retrograde transport to the cell bodies (Fig. 3Ai inset, Bii, Cii). During episodes of fictive locomotor activity, visible as rhythmic bursting in the spinal VR (green trace in Fig. 3Ai), the population of tentacle motoneurons showed fluorescence changes that were timed to the VR bursting (Fig. 3Ai). Simultaneous Ca^{2+} imaging of the bilateral tentacle motor nuclei (red and blue outline in Fig. 3Ai inset) yielded almost identical dynamics of the transients (red and blue traces in Fig. 3Ai), matching the symmetric motion profiles of the two appendages (Fig. 1Ci,D). The duration of these population responses (*n*=15 swimming episodes in *N*=8 preparations), measured as half-width of the Ca^{2+} transients (Fig. 3Ai), was highly correlated with the

The Journal of Experimental Biology (2015) 218, 1748-1758 doi:10.1242/jeb.120824

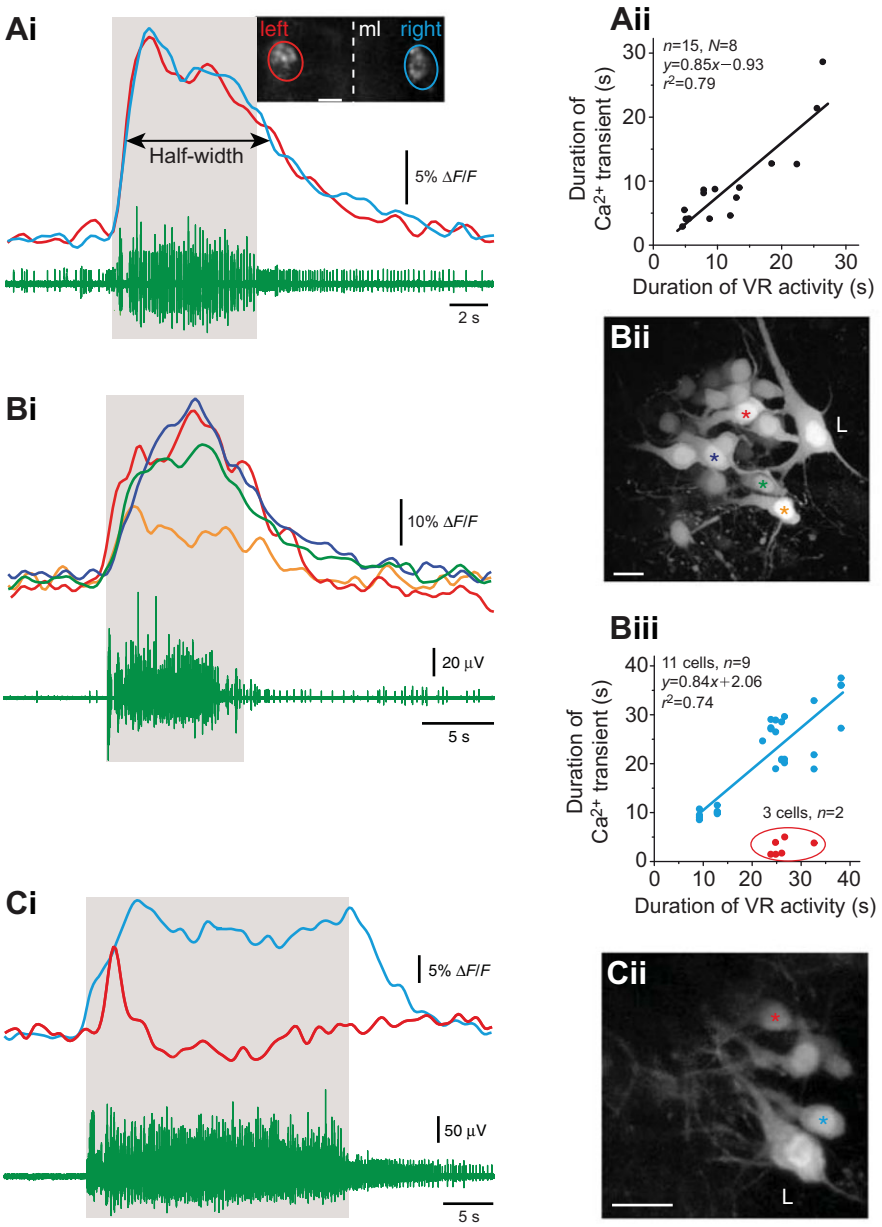

Fig. 3. Calcium dynamics in tentacle motoneurons during fictive locomotion. (Ai) Population Ca^{2+} transients (red and blue traces) of the tentacle motor nuclei on both sides (red and blue encircled areas in inset) during an episode of fictive swimming (gray area), indicated by the spinal ventral root (VR) burst discharge (green trace); motoneurons were retrogradely labeled with the Ca^{2+} sensor (Calcium Green-1 dextran) from the target muscle. (Aii) Scatter plot and linear regression of population Ca^{2+} response duration (half-width) as a function of the duration of rhythmic VR activity during n=15 swimming episodes in N=8 preparations (r^2=0.79, P<0.0001, Wilcoxon signed-rank test). (B,C) Ca^{2+} transients (color-coded traces in Bi, Ci) of individual tentacle motoneurons (color-matched asterisks in Bii, Cii) during episodes of fictive swimming (gray areas in Bi, Ci). (Biii) Scatter plot and linear regression of the Ca^{2+} response half-width in single neurons (blue dots) as a function of the duration of rhythmic VR activity (r^2=0.74, P<0.0001, Wilcoxon signed-rank test); note the small group of motoneurons (red dots) with highly phasic Ca^{2+} transients (red trace in Ci) during fictive swimming (no significant correlation, P>0.05). Data in B and C are from 14 cells during n=9 swimming episodes in N=3 preparations (31 data points). L, large neurons (see Fig. 2D); ml, midline. Scale bars are 100 µm in inset of Ai, 20 µm in Bii and Cii.

duration of the fictive swimming episodes (Fig. 3Aii). Thus, the duration of Ca^{2+} responses in the tentacle motor nuclei closely matches the duration of a swimming episode.

In a separate set of experiments, we determined the fraction and morphology of the activated tentacle motoneurons by recording Ca^{2+} responses of individual motoneurons (34 cells; n=9 swimming episodes in N=3 preparations; Fig. 3Bii,Cii). Ca^{2+} transients were encountered in 14 out of 34 retrogradely identified motoneurons during fictive swimming episodes (Fig. 3Bi,Ci). Responses were observed only in the population of medium-sized motoneurons with oval cell bodies (16.1±1.6 µm, 14 cells), whereas neither the subgroup of small motoneurons nor the one to two very large motoneurons displayed any locomotion-related responses (Fig. 3B,C). Based on the dynamics of the Ca^{2+} responses, the 14 responsive neurons could be separated into a majority of cells (11 cells; color-coded traces in Fig. 3Bi and blue trace in Fig. 3Ci) with a half-width of the transients that significantly correlated with the duration of the corresponding swimming episode (blue dots in Fig. 3Biii). In contrast, a few motoneurons (two swimming episodes in three neurons) exhibited Ca^{2+} responses that were highly transient and only present at the beginning of a swimming episode (red trace in Fig. 3Ci; red dots in Fig. 3Biii). However, the morphology of these neurons was indistinguishable and the size not significantly different from the size of those with the predominant response pattern. Thus, motoneurons responsible for tentacle motion during tadpole swimming appear to form a morphologically homogeneous group with Ca^{2+} response profiles that suggest the presence of either transient or sustained activity during locomotor episodes.

Dynamics of tentacle motor commands

To reveal the discharge profile of the motor commands that provoke tentacle movements during locomotor CPG activity, we made simultaneous recordings of a VR on one or both sides of the spinal cord, the TN on one side and the motion of the tentacle on the other side (Fig. 4A). During fictive swimming, indicated by an episode of burst activity in VRs (green and gray traces in Fig. 4B), the otherwise silent TN became active (black trace and firing rate

The Journal of Experimental Biology (2015) 218, 1748-1758 doi:10.1242/jeb.120824

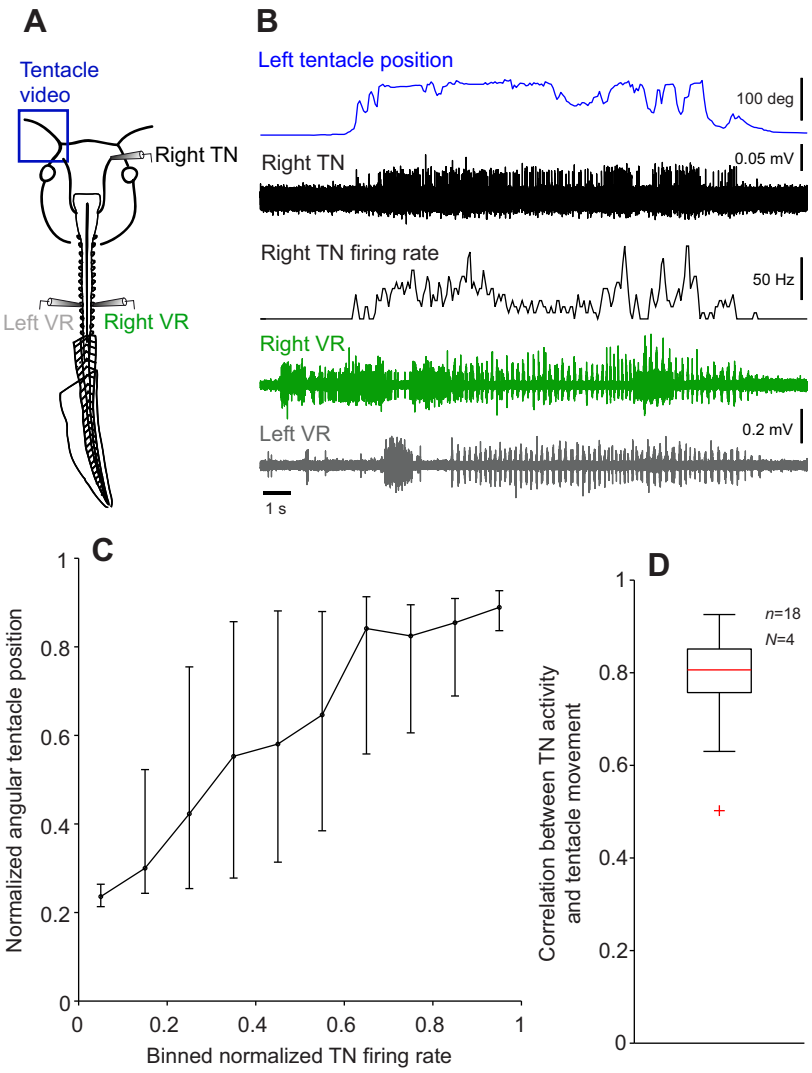

Fig. 4. Correlation between TN motoneuronal activity and tentacle movement during fictive locomotion. (A) Sketch depicting simultaneous video imaging of the left tentacle and electrophysiological recording of the right TN and bilateral spinal VRs in a semi-intact tadpole preparation. (B) Tentacle motion (blue trace), TN spike activity and instantaneous firing rate (black traces) and bilateral VR discharge (green and gray traces) during fictive swimming. (C) Median and 25th and 75th percentiles of normalized tentacle position plotted against normalized and binned TN firing rate of n=18 swimming episodes in N=4 preparations. (D) Boxplot illustrating the distribution of the correlation coefficients between the firing rate of the TN on one side and the movement of the tentacle on the other side (red cross indicates outliers) for the swimming episodes in C with a median of 0.81 (the distribution is significantly different from zero, P<0.001; Wilcoxon signed-rank test).

in Fig. 4B). In addition, the intact tentacle contralateral to the recorded TN was simultaneously retracted (blue trace in Fig. 4B). The similarity of tentacle motion and tentacle motor profiles (blue and black traces in Fig. 4B) was quantified by correlating the normalized position of the tentacle with the normalized firing rate of the contralateral TN (Fig. 4C). Normalized tentacle motion and contralateral TN firing rates were correlated with a coefficient ranging between 0.50 and 0.93 (median: 0.81; n=18 swim episodes in N=4 preparations; Fig. 4D). The distribution of correlation coefficients was significantly different from zero (P<0.001; Wilcoxon signed-rank test). Despite the variability in the movements of both tentacles (Fig. 1Ci), the distribution of correlation coefficients indicates that the firing pattern of the TN on one side faithfully predicts the motion profile of the tentacle on the other side.

Coupling properties of locomotor and tentacle motor activity

Locomotor influence on tentacle motion was studied by analyzing the coupling pattern between spinal and tentacle motor activity. Tadpole swimming is a fluctuating motor behavior in terms of duration and strength/speed, which is reflected during fictive locomotion by variable episode durations, burst frequencies and amplitudes (Combes et al., 2004). By comparing spinal VR and TN activity, we identified those parameters of the locomotor commands that are transmitted to the tentacle motor system. The most obvious of these parameters was the duration of the fictive swimming episode: the discharge in spinal VRs and in the TN closely matched in time (compare black with green traces in Fig. 5A), as indicated by the significant linear regression with a slope close to unity (Fig. 5B; r^2=0.94, P<0.0001, Wilcoxon signed-rank test, n=57 swim episodes in N=10 preparations). This agrees with the behavioral observation that the tentacles are retracted during the entire swimming event.

Alterations in swimming strength *in vivo* essentially derive from changes in the magnitude and frequency of tail excursions that in turn are represented *in vitro* by variations in the cycle frequency of the VR bursts and in the intra-burst firing rate (Combes et al., 2004). A spontaneous increase in spinal VR intra-burst discharge, represented by a larger integral of the firing rate (green traces in Fig. 5C) was accompanied by a similar increase in retraction angle of the tentacle (blue trace in Fig. 5C). With increasing locomotor strength from low to medium to high swimming amplitudes (Fig. 5D), the tentacle reached progressively more eccentric positions. In fact, the tentacle positions for the three levels of swimming strength were significantly different from each other (P<0.0001, Kruskal–Wallis test and *post hoc* comparisons; n=4 swimming episodes in N=3 preparations). The variation of position with swimming strength prompted us to compare the swimming

The Journal of Experimental Biology (2015) 218, 1748-1758 doi:10.1242/jeb.120824

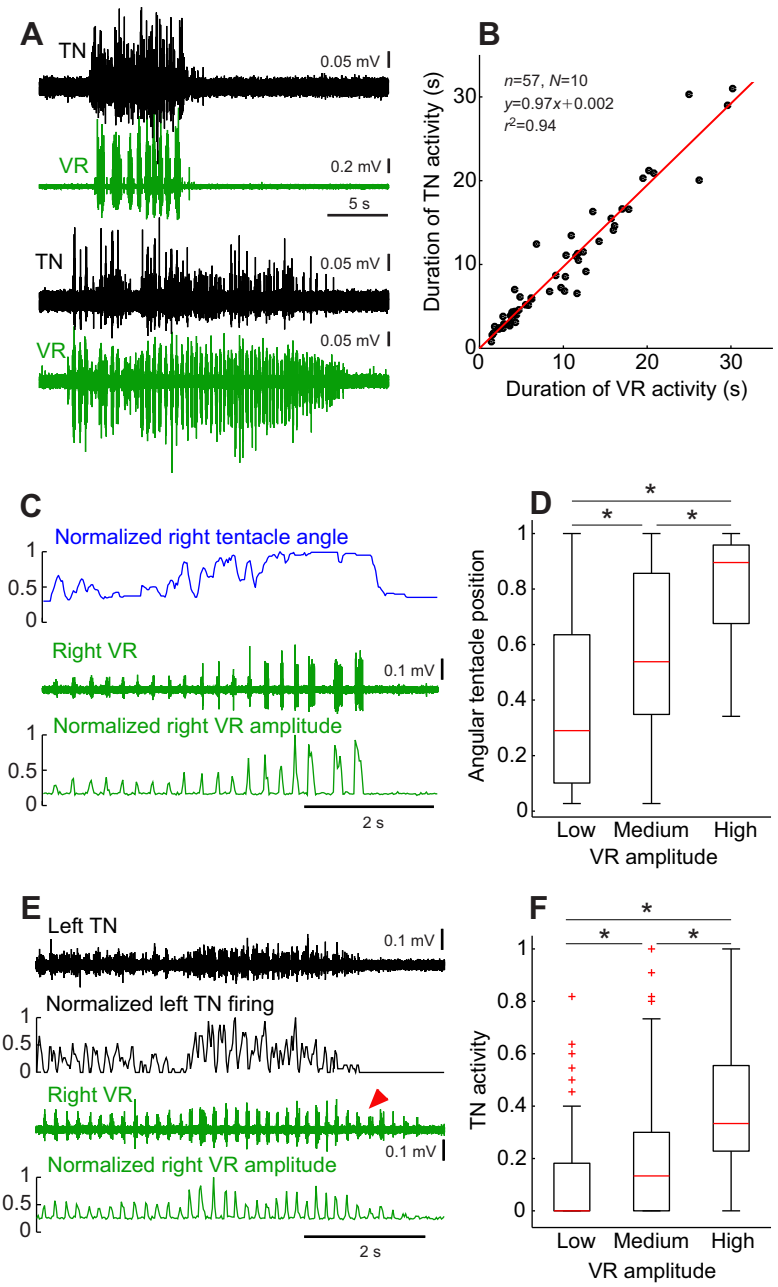

Fig. 5. Tentacle motor commands contain information about fictive swimming duration and amplitude. (A) TN discharge (black traces) and VR burst activity (green traces) during two fictive swimming episodes of different length in the same preparation. (B) Scatterplot and linear regression of TN discharge duration as a function of the duration of VR activity during n=57 swimming episodes in N=10 preparations (r^2=0.94). (C) Angular trajectory of the tentacle (normalized to maximal excursion, blue trace), ipsilateral VR activity with increasing burst amplitude (upper green trace) and integrated burst amplitudes (normalized to maximal value, lower green trace) during an episode of fictive swimming. (D) Boxplot of tentacle angular position as a function of VR burst amplitude; normalized VR burst amplitudes were binned into three levels (low, medium and high); normalized tentacle angular positions, obtained from n=4 swimming episodes in N=3 preparations, were significantly different between the three groups (P<0.0001; Kruskal–Wallis test and *post hoc* comparisons). (E) TN discharge (upper black trace), contralateral VR burst activity (upper green trace) and normalized TN and VR firing rate amplitudes (to maximal magnitude; lower black and green traces, respectively) during fictive swimming with modulated VR burst amplitudes. (F) Boxplot (red crosses indicate outliers) of TN firing rate as a function of VR burst amplitude; normalized VR burst amplitudes were binned into three levels (low, medium and high); normalized TN firing rate amplitudes – obtained from n=4 swimming episodes in N=3 preparations – were significantly different between the three groups (P<0.0001, Kruskal–Wallis test and *post hoc* comparisons).

strength (green traces in Fig. 5E) during a given locomotor episode with the rate of TN firing (black traces in Fig. 5E). Spontaneous alterations of VR burst amplitude caused a comparable modulation of the TN firing rates, with the latter discharge ceasing as soon as the VR bursting decreased below a particular level (red arrowhead in Fig. 5E). Pooling the data from four different swimming episodes in three preparations where the VR burst discharge frequency displayed a spontaneous modulation showed that the TN activities at the three levels of swimming strength were also significantly different from each other (Fig. 5F; P<0.0001, Kruskal–Wallis test with *post hoc* comparisons), with a more pronounced TN activity during stronger swimming.

While the previously described corollary discharge in extraocular motoneurons during rhythmic locomotion in *Xenopus* tadpoles is strictly phase coupled to the VR bursting in a 1:1 fashion (Lambert et al., 2012), the dynamics of tentacle motor commands appears to be more variable and temporally more complex (Fig. 6). To assess the coupling of TN spiking during episodes of fictive swimming as a function of the timing of VR bursts, we generated VR burst-triggered cumulative spike time histograms (see Materials and methods). Based on entropy statistics (Kajikawa and Hackett, 2005), recordings from 18 out of 31 swimming episodes in N=7 preparations (58%) showed significant phase coupling between spinal VR and TN discharge (Fig. 6A,B,D), while the TN discharge during 13 swim cycles displayed no coupling to the VR burst rhythm (Fig. 6C). In the group of phase-coupled recordings, a mono-phasic coupling (four out of 18; Fig. 6A) could be clearly distinguished from a bi-phasic pattern (five out of 18; arrowhead in Fig. 6Bii inset), while the remainder (nine out of 18) exhibited a phase coupling that could not be unambiguously distinguished as one or the other. The different coupling patterns during individual swimming bouts were summarized as circular plots, emphasizing the variability among the different coupling categories (Fig. 6Aiii–Ciii). Functionally, the mono- or bi-phasic timing of TN bursts (Fig. 6Aiii, Biii) suggests that

The Journal of Experimental Biology (2015) 218, 1748-1758 doi:10.1242/jeb.120824

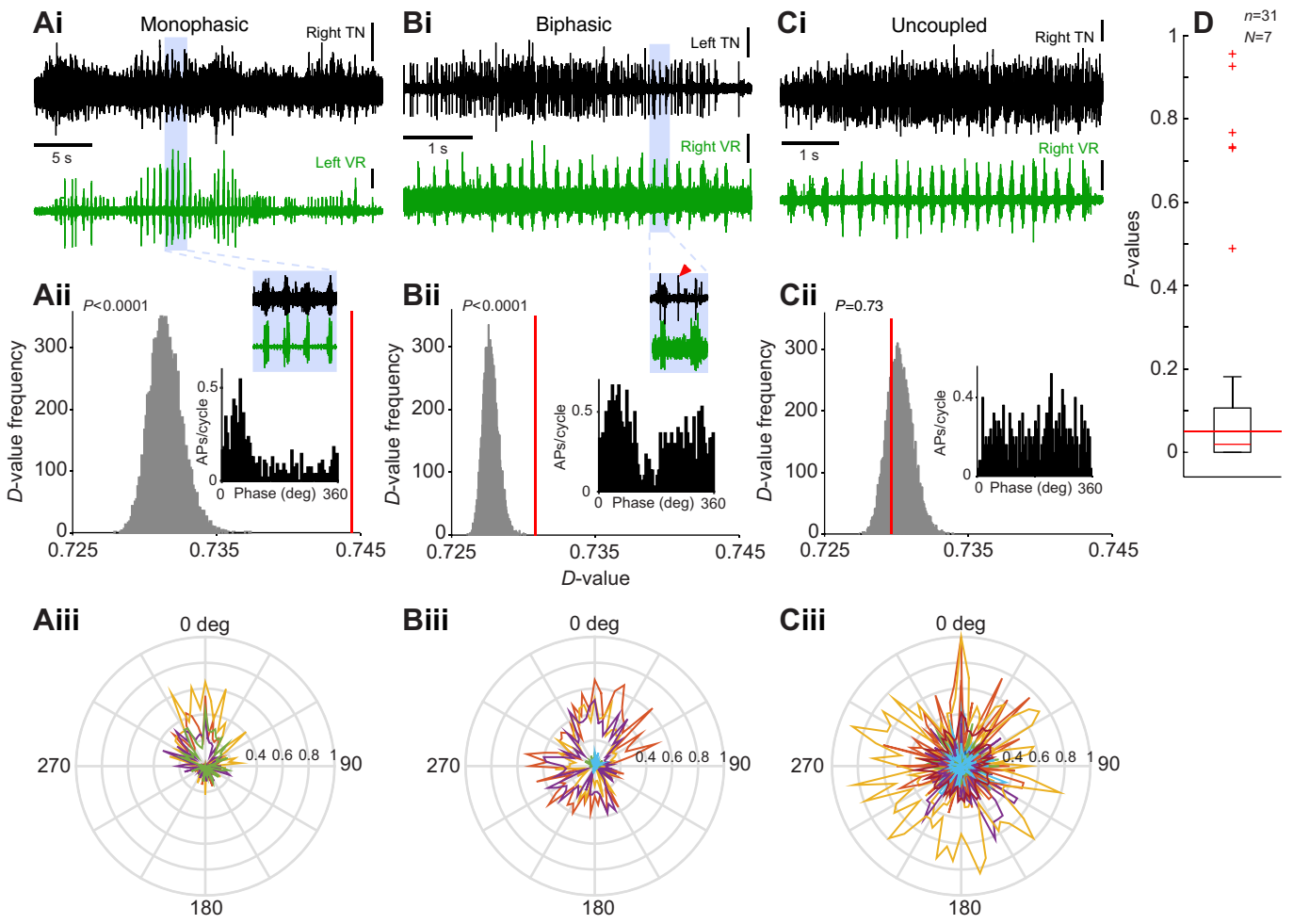

Fig. 6. Phase coupling between TN and VR activity during fictive locomotion. (A–C) TN discharge (black traces) and contralateral (Ai, Bi) or ipsilateral (Ci) VR burst activity (green traces); VR–TN coupling subdivides into mono-phasic (Ai), bi-phasic (red arrowhead in Bi) and uncoupled patterns (Ci) as indicated by the insets on an extended time scale (blue background); distribution of *D*-values (Aii, Bii, Cii) from re-shuffled inter-spike intervals (see Materials and methods) in the TN recording from the three examples (Ai, Bi, Ci) assessed the significance of phase coupling; the *D*-value from the original trace is indicated by the red vertical line; insets in Aii, Bii and Cii show the spike histograms of the TN discharge relative to the swimming phase. Circular plots in Aiii, Biii and Ciii summarize the distribution of TN spikes across VR cycles for individual swimming bouts (color coded). (D) Boxplot of the *P*-value distribution obtained from *n*=31 swimming episodes in *N*=7 preparations to assess the significance of phase coupling based on the *D*-value. Scale bars: Ai TN, 0.05 mV; VR, 0.2 mV, Bi TN, 0.2 mV; VR, 0.05 mV, Ci TN, 0.05 mV; VR, 0.1 mV.

the inputs to trigeminal motoneurons originate from one or both sides of the spinal cord during a particular recording. This might also explain the difficulty of assigning a particular phase relation to the coupling pattern in most cases (mono- versus bi-phasic), assuming a continuum between unilateral and bilateral locomotor corollary drive to tentacle motoneurons.

DISCUSSION

During fictive swimming in *Xenopus* tadpoles, a corollary discharge informs the tentacle motor system about ongoing locomotor activity. This intrinsic locomotor signal activates a discrete set of trigeminal motoneurons on each side of the rostral hindbrain that causes a symmetrical retraction of the appendages. The motor command encodes both duration and magnitude of the locomotor activity, thereby ensuring a reliable coupling between propulsive locomotion and tentacle motion. Given the phase coupling between trigeminal nerve discharge and spinal motor rhythm, the locomotor corollary discharge derives at least in part from the spinal central pattern generator (CPG) circuitry.

Function of tentacles

Xenopus laevis tadpoles possess a pair of mobile appendages between developmental stage 47 and 61 (Nieuwkoop and Faber, 1994), which contain Merkel cells and thus were suggested to play a role in touch reception (Ovalle, 1979; Ovalle et al., 1998). These tentacles are usually protruded forward but can be actively retracted into a lateral position (Fig. 1A). The use of appendages for mechanoreceptive exploration of the environment in these animals is useful for near-field orientation and navigation in the mostly murky aquatic environment in which these animals naturally live (Nieuwkoop and Faber, 1994). A similar mechanoreceptive role in mammals is performed by mechanoreceptive facial hairs – whiskers. Rodents use whisker movements for tactile exploration of the environment, for instance while walking along the wall of a cage (Hartmann, 2011). Similarly, tadpoles drift slowly with their tentacles touching the walls and floor of the tank (S.H., R.B., H.S. and B.P.C., unpublished observation), potentially collecting tactile information. However, several differences between the two structures exist: tentacles are formed by a single protrusion located on each side of the head, while whiskers are usually arranged in

The Journal of Experimental Biology (2015) 218, 1748-1758 doi:10.1242/jeb.120824

groups (Berg and Kleinfeld, 2003). Moreover, whisker movements in rodents are controlled by multiple muscles (Berg and Kleinfeld, 2003), while tentacle motion in *Xenopus* tadpoles is exerted by a single muscle and a spring-like antagonistic mechanism (Ovalle et al., 1998). For tactile exploration, whiskers are actively moved ('whisking'), while tentacles are kept in an extended position. However, despite these morphological differences, amphibian tentacles appear to be similar, yet simpler versions of touch-receptive mammalian appendages.

Potential function of tentacle retraction

The presence of Merkel cells at a relatively high density in *Xenopus* tentacles (Ovalle, 1979) indicates a particular sensitivity of these structures to touch. Because of the hydrodynamic drag between the appendages and water, permanently extended tentacles could rhythmically stimulate these touch receptors during swimming-related head undulations. A tonic retraction of the tentacles during locomotor episodes might considerably reduce excessive stimulation of the sensory cells, in particular during strong and fast swimming. Under this assumption, locomotor corollary discharge-mediated tentacle retraction would minimize self-generated stimulation of the Merkel cells during swimming by reducing the water flow/pressure impinging on the tentacles. In a number of other sensory systems, corollary discharge similarly reduces or even suppresses self-generated sensory inputs (for review, see Crapse and Sommer, 2008); this also complies with the classical role of motor efference copies or corollary activity (von Holst and Mittelstaedt, 1950; Sperry, 1950). As a side effect, tentacle retraction during locomotion reduces the likelihood of mechanical damage to the tentacles that can reach a maximal length of 1 cm (~20% of larval body length).

In addition to this putative protective function, tentacle retraction might also improve the hydrodynamics of the tadpole. Appendage retraction streamlines the body shape, thereby facilitating energetically more efficient swimming (Crespi et al., 2013; Liu et al., 1997). This is particularly important during strong swimming, when protruded tentacles would cause a considerable drag and impair the sinusoidal motion of the head during swimming, specifically at those larval stages where these appendages are at their maximal length. In fact, a similar streamlining of the body shape is observed during tail-based swimming in other amphibians such as salamanders, where both forelimbs and hindlimbs are aligned to the body (Delvolvé et al., 1997) or in axolotl, where the external gills are retracted (D'Août and Aerts, 1997). Thus, locomotor-coupled head appendage or limb retractions in amphibians represent distinct behavioral reactions that improve the hydrodynamic signature and, in the case of retracted limbs during tail-based swimming, considerably enhance locomotor performance (Crespi et al., 2013). Such a strategy is not restricted to amphibians but occurs also during swimming in alligators (Manter, 1940; Fish, 1984) and 'terrestrial swimming' in sandfish lizards (Maladen et al., 2009) where the tail-based propulsion is accompanied by similar limb adductions as in salamanders (Delvolvé et al., 1997).

Origin of corollary discharge in trigeminal/tentacle motoneurons

The absence of propulsive movements and movement-related sensory feedback in semi-intact *Xenopus* preparations (Straka and Simmers, 2012) demonstrates that the coupling between locomotion and tentacle motion relies exclusively on intrinsic signals, i.e. corollary discharge from locomotor areas. Theoretically, these signals could derive from midbrain locomotor centers (Cabelguen et al., 2003; Saitoh et al., 2007) or from CPGs in the rostral spinal cord or from a combination of the two.

A spinal contribution of the corollary activity in tentacle motoneurons is supported by the presence of strict phase coupling of the TN burst discharge with the burst rhythm of the spinal VR on one (mono-phasic) or on both sides (bi-phasic; Fig. 6A,B) along with the highly correlated amplitudes of spinal VR and TN firing or tentacle motion. The absence of a clear VR–TN burst coupling in a number of experiments (Fig. 6C) might reflect the consequence of signal integration in a particular motoneuronal population that only becomes apparent in some experiments depending on the number and variety of recorded TN axons. Alternatively, or in addition, the ascending spinal locomotor corollary discharge in tentacle motoneurons, unlike in extraocular motoneurons (Lambert et al., 2012) might be supplemented by tonic signals from locomotor centers in the midbrain and/or hindbrain. In fact, midbrain neurons in the salamander *Notophthalmus viridescens*, for instance, display tonic activity during locomotion (Cabelguen et al., 2003), similar to that seen in the TN nerve during locomotor episodes. Even though the relative contributions of midbrain locomotor regions and spinal CPGs to the tentacle motor corollary discharge remain unclear, we hypothesize that both neuronal structures contribute to the trigeminal activation during locomotor activity.

Evolutionary origin of spinal–hindbrain coupling

While locomotion-related tentacle retraction potentially serves several distinct, not mutually exclusive purposes (see above), the coupling could be a vestige of the rostro-caudally distributed activity in the spinal cord-like nervous system of vertebrate ancestors during undulatory swimming (Fetcho, 1992; Wada, 1998). However, given the rather specialized structure and function of these rostral appendages, this notion appears too simplistic. The inherent linkage between the two motor systems rather suggests a particular functional role of tentacle retraction during swimming, which is not necessarily exclusive or in opposition with a pre-existing vestigial signaling pathway. Accordingly, ascending locomotor corollary discharges from the spinal CPG circuitry might represent a widely distributed signaling component within the brain during rhythmic locomotion and might influence numerous sensory and/or motor systems. Among the hindbrain motor systems currently known to receive spinal inputs are the extraocular system (Combes et al., 2008; Lambert et al., 2012; von Uckermann et al., 2013) and the trigeminal motor component (this study). Evidence for an even more widespread function arises from studies on spiny dogfish (Russell and Roberts, 1974) and larval *Xenopus* (Chagnaud et al., 2012b), in which connections from the spinal cord locomotor CPG to mechanosensory efferent neurons were demonstrated. Further hindbrain targets might include hindbrain nuclei in axolotl that cause a retraction of the gills during swimming (D'Août and Aerts, 1997).

Based on the various examples, we hypothesize that appendage retraction (e.g. limbs, tentacles, gills) during undulatory swimming is generally caused by locomotor corollary activity, which allows a fast and reliable coupling of independent motor behaviors with locomotion. Such a functional role expands the traditional concept of motor efference copies/corollary discharge in simply differentiating between external and self-generated sensory signals (Cullen, 2004, 2011). Accordingly, corollary discharge during locomotor activity appears to influence a large number of both sensory and motor systems throughout the brain, including the

The Journal of Experimental Biology (2015) 218, 1748-1758 doi:10.1242/jeb.120824

trigeminal system, potentially optimizing locomotor performance and sensory perception (Chagnaud et al., 2012a). Depending on the type of motor behavior (rhythmic, task oriented), the effect of corollary activity might vary considerably (Crapse and Sommer, 2008; Cullen, 2014; King, 2013). Nonetheless, intrinsic coupling offers a convenient substrate for a context-dependent, direct linkage between otherwise discrete motor behaviors.

MATERIALS AND METHODS

Experiments were performed on semi-intact *in vitro* preparations of 33 larval *Xenopus* at stages 51–55 (Nieuwkoop and Faber, 1994) in compliance with the 'Principles of Animal Care' publication by the National Institutes of Health and the German law for animal protection (Tierschutzgesetz). Permission for the experiments was granted by the Regierung von Oberbayern (55.2-1-54-2531.3-18-10). All animals were obtained from the in-house breeding facility at the Biocenter-Martinsried of the LMU Munich.

Preparations

In all experiments, animals were first anesthetized in 0.02% 3-aminobenzoic acid ethyl ester (MS-222; Sigma-Aldrich Pharma Ltd, UK) in ice-cold frog Ringer solution (composition in mmol l^{-1}: NaCl, 75; KCl, 2; $CaCl_2$, 2; $MgCl_2$, 0.5; $NaHCO_3$, 25; glucose, 11: pH 7.4). The ventral part of the head/body, including the lower jaw and visceral organs, was carefully removed, leaving the tail attached to the head and the sensory-motor innervation of the tentacles intact. The skin covering the dorsal portion of the head was removed, the soft skull tissue opened and the forebrain disconnected. Preparations were transferred to a Petri dish (volume 5 ml) and fixed dorsal-side up to the Sylgard floor with insect pins. In some cases the spinal cord was exposed up to segment 20 and the VRs were transected bilaterally. The remaining, caudal part of the tail was firmly secured on both sides to the Sylgard floor with insect pins at the level of segments 21–25, with the remainder of the tail left free to perform undulatory swimming movements. After repeated rinsing in fresh Ringer solution, preparations were continuously superfused with oxygenated Ringer solution at a rate of 1.3–2.1 ml min^{-1}. The temperature of the bath solution was maintained at 17±0.5°C. Recordings lasted up to 5 h.

Tentacle motor behavior during spinal VR activity (i.e. fictive swimming, hereafter referred to as swimming) in these isolated preparations was quantified by video analyses of tentacle motion and/or recording the respective motor nerve discharge. For monitoring tentacle movements during fictive swimming, one or both tentacle(s) remained attached and innervated by the respective trigeminal nerve branch. Motor commands for tentacle movements were captured after further unilateral or bilateral isolation of the trigeminal motor nerve branch that innervates the tentacle muscle.

Behavioral analysis of tentacle motion

Movements of one or both tentacles during spinal locomotor activity (see below) were video-captured from the top in isolated preparations (n=8) with a CCD camera (Axiocam, Zeiss, Germany) with a resolution of 272×208 pixels at a rate of 20–50 frames s^{-1} either separately or in combination with the spike activity of the contralateral tentacle motor nerve. The motion trajectory of the tentacle was analyzed offline by manually tracking the distal yet still straight portion of the tentacle with respect to the base using the Vidana software (courtesy of Dr M. Hofmann). From the position coordinates, the angle of the tentacle relative to the longitudinal body axis was calculated in Matlab (MathWorks, Natick, MA, USA) and plotted as motion trajectory over time.

Electrophysiological recordings

Spontaneous or evoked locomotion in isolated tadpole preparations was recorded as bilaterally alternating rhythmic burst discharge in spinal VRs, termed fictive swimming (e.g. Combes et al., 2004). Multi-unit activity from one or two spinal VRs of segments 10–15 along with the discharge of one or both tentacle motor nerves (N=12) were recorded with individually adjusted glass suction electrodes, fabricated with a horizontal puller (P-97 Brown/Flaming, Sutter Instruments, Novato, CA, USA). The recorded neuronal activity was amplified (EXT 10-2F; npi electronics, Tamm, Germany), digitized at 10 kHz (CED 1401, Cambridge Electronic Design, Cambridge, UK), processed with commercial software (Spike 2, Cambridge Electronic Design), stored on a PC and analyzed off-line with custom-written scripts using Igor Pro (Wavemetrics, Tigard, OR, USA) or Matlab.

Data analysis

To compare the tentacle retraction on one side with the TN firing on the other side, we calculated the correlation coefficient after normalizing the angular tentacle position and the TN firing rate to their maximum for each swimming bout. The temporal relationship between rhythmic spinal VR and trigeminal motor activity was evaluated by comparing the duration of the concurrent discharge episodes, obtained from multi-unit recordings of at least one VR and one TN. These data were extracted from n=57 individual swimming episodes (these included only rhythmic alternating activity and no escape) in N=10 preparations and compared using a scatter plot and linear regression.

The degree and variation of swimming strength during fictive locomotion were estimated from integrals of the VR bursting in recordings of those locomotor episodes that showed a modulation of the swimming strength. In these traces, the swimming amplitude was calculated from integrals of VR bursts with a bin width of 30 ms (N=2 preparations) or with a bin width that matched the frame rate of simultaneously video-recorded tentacle motion (21 ms, N=3 preparations; 71 ms, N=1 preparation). Integrated and binned VR burst amplitudes were normalized to the maximal magnitude within a given swimming episode and were grouped according to amplitude into three categories (low, medium, high) indicating weak, medium and strong swimming. These three different levels were used to plot the normalized firing rate of the simultaneously recorded TN or the video-recorded tentacle position. Significance between the three levels was tested using a Kruskal–Wallis test, followed by *post hoc* multiple sample comparisons (Wilcoxon signed-rank tests).

To determine potential phase correlations between swimming (i.e. VR activity) and TN activity, the instantaneous firing rate of the VR bursts was calculated from recordings of 31 locomotor episodes in N=7 preparations. The phase relationship between the TN discharge and VR bursts was calculated and plotted as a histogram of spikes with a bin size of 5 deg (one burst cycle=360 deg). The histogram was normalized by dividing the spike count by the number of swimming cycles. Histogram data were displayed as circular plots, with their maxima aligned at 0 deg. To assess whether the distribution of spikes in the TN was phase coupled to unilateral or bilateral VR activity, a previously described procedure was employed (Kajikawa and Hackett, 2005). Briefly, the entropy (D score) of the plotted spike time histogram was calculated as the difference between unity and a normalized entropy measure (D=1−E/E_{max}). D may vary from 0 to 1, with 0 being no phase coupling (probability of firing is equally distributed over the entire swimming cycle) and 1 being maximal phase coupling, independent of the underlying spike time distribution. In order to determine the significance of D, the inter-spike intervals were reshuffled 10,000 times for each swimming episode and a D-value was calculated for each repetition (Kajikawa and Hackett, 2005). The D-value from the initial analysis was then compared with this distribution of reshuffled D-values by calculating the proportion of those that were equally large or larger than the original value. Phase coupling was considered significant if this proportion was smaller than 0.05 (i.e. one-tailed probability with α=0.05).

Anatomical identification of tentacle motoneurons

To assess the location and spatial arrangement of tentacle motoneurons in the hindbrain, fluorescent tracers (Alexa Fluor dextran 488, 546; Life Technologies, Carlsbad, CA, USA) and biocytin (Sigma-Aldrich) were applied to different portions of the trigeminal nerve in isolated *in vitro* preparations (Straka et al., 2001). Crystals of the respective tracer, melted

to the tip of an injection needle, were inserted into various trigeminal nerve branches or the main trigeminal nerve root. After overnight incubation in oxygenated Ringer solution at 14°C, preparations were fixed in 4% paraformaldehyde in 0.1 mol l^{-1} phosphate buffer (PB, pH 7.4) at 10°C for 5–12 h and rinsed (3×10 min) in cold 0.1 mol l^{-1} phosphate-buffered saline (PBS, pH 7.4). In experiments where biocytin was applied, preparations were fixed and rinsed as described above and kept in Dent's solution [80% methanol, 20% dimethylsulfoxide (DMSO)] at room temperature for 12–14 h, transferred into 100% methanol and stored at −80°C for at least 1 h. Then, preparations were rehydrated at room temperature in 70%, 50% and 35% methanol solutions in distilled water for 1 h each, followed by 0.1 mol l^{-1} PBS (3×30 min), incubated in a 1:200 solution of streptavidin-Cy2 (Dianova, Germany) in 0.1 mol l^{-1} PBS for 2 h and rinsed in PBS (3×30 min). The brainstem of all preparations was removed, cleaned of surrounding tissue, mounted on slides and coverslipped with Vectashield (Vector Laboratories, Burlingame, CA, USA). Retrogradely labeled neurons and afferent nerve terminations were reconstructed from stacks of optical sections (1.5–3 µm) obtained from a confocal microscope (SP5, Leica, Germany). In order to map the position of retrogradely labeled motoneurons onto the rhombomeric scaffold, preparations were additionally scanned with an illumination wavelength of 633 nm, outlining the spatial arrangement of the rhombomeres (r). *Z*-axis projections, image processing and quantification of neuronal numbers were carried out using the Fiji software package (http://fiji.sc/wiki/index.php/Fiji).

Imaging of Ca^{2+} transients in tentacle motoneurons

Tentacle motoneurons were retrogradely labeled 1–2 days prior to the experiment with Calcium Green-1 dextran (Life Technologies) by applying crystals of this Ca^{2+} sensor to the peripheral part of the tentacle motor nerve. Imaging of Ca^{2+} transients was performed with a confocal scanning microscope (LSM 700, Carl Zeiss, Germany) in the presence and absence of fictive locomotor activity. To prevent potential movement artifacts during imaging, all residual muscular elements of the isolated preparation were removed, except for the most caudal portion of the tail, which was left free to perform swimming movements (see above). Images were acquired at a rate of 5–10 frames s^{-1} (ZEN black, Carl Zeiss, Germany), stored and analyzed *post hoc*. Image analysis was performed off-line using the Fiji software package and custom-written scripts in Igor Pro. Background fluorescence was subtracted and bleaching was corrected using a linear regression algorithm. All data are presented as relative changes in fluorescence ($\Delta F/F$). The duration of Ca^{2+} transients were determined as the time at half-maximal amplitude of the fluorescence change (half-width) during a given swimming episode.

Acknowledgements

The authors thank Dr M. Hofmann for the Vidana software and D. Wickmaier for contributions to initial experiments.

Competing interests

The authors declare no competing or financial interests.

Author contributions

S.H., R.B., H.S. and B.P.C. planned the experiments, S.H., R.B. and B.P.C. acquired and analyzed the data, S.H., R.B., H.S. and B.P.C. wrote the manuscript.

Funding

Financial support was provided by the German Science Foundation [CRC870 to B.P.C. and H.S.; RTG1373 to R.B.] and the Graduate School of Systemic Neurosciences [to S.H.].

References

Berg, R. W. and Kleinfeld, D. (2003). Rhythmic whisking by rat: retraction as well as protraction of the vibrissae is under active muscular control. *J. Neurophysiol.* **89**, 104-117.

Bramble, D. and Carrier, D. (1983). Running and breathing in mammals. *Science* **219**, 251-256.

Cabelguen, J.-M., Bourcier-Lucas, C. and Dubuc, R. (2003). Bimodal locomotion elicited by electrical stimulation of the midbrain in the salamander *Notophthalmus viridescens*. *J. Neurosci.* **23**, 2434-2439.

Cannone, A. and Kelly, P. (1977). The tentacles of *Xenopus laevis* tadpoles - evidence for a mechanoreceptive role. *S. Afr. Med. J.* **52**, 407.

Chagnaud, B. P., Simmers, J. and Straka, H. (2012a). Predictability of visual perturbation during locomotion: implications for corrective efference copy signaling. *Biol. Cybern.* **106**, 669-679.

Chagnaud, B. P., Banchi, R. and Straka, H. (2012b). Spinal corollary discharge informs mechanoreceptor organs about frequency and duration of locomotor activity. In *Neuroscience 2012 Abstracts* (ed. S. F. Neuroscience). New Orleans: online, 470.01.

Combes, D., Merrywest, S. D., Simmers, J. and Sillar, K. T. (2004). Developmental segregation of spinal networks driving axial- and hindlimb-based locomotion in metamorphosing *Xenopus laevis*. *J. Physiol.* **559**, 17-24.

Combes, D., Le Ray, D., Lambert, F. M., Simmers, J. and Straka, H. (2008). An intrinsic feed-forward mechanism for vertebrate gaze stabilization. *Curr. Biol.* **18**, R241-R243.

Crapse, T. B. and Sommer, M. A. (2008). Corollary discharge across the animal kingdom. *Nat. Rev. Neurosci.* **9**, 587-600.

Crespi, A., Karakasiliotis, K., Guignard, A. and Ijspeert, A. J. (2013). Salamandra robotica II: an amphibious robot to study salamander-like swimming and walking gaits. *IEEE Trans. Robotic.* **29**, 308-320.

Cullen, K. E. (2004). Sensory signals during active versus passive movement. *Curr. Opin. Neurobiol.* **14**, 698-706.

Cullen, K. E. (2011). The neural encoding of self-motion. *Curr. Opin. Neurobiol.* **21**, 587-595.

Cullen, K. E. (2014). The neural encoding of self-generated and externally applied movement: implications for the perception of self-motion and spatial memory. *Front. Integr. Neurosci.* **7**, 108.

D'Août, K. and Aerts, P. (1997). Kinematics and efficiency of steady swimming in adult axolotls (*Ambystoma mexicanum*). *J. Exp. Biol.* **200**, 1863-1871.

Davis, W. J., Mpitsos, G. J. and Pinneo, J. M. (1974). The behavioral hierarchy of the mollusk *Pleurobranchaea*. *J. Comp. Physiol. A* **90**, 225-243.

Delvolvé, I., Bem, T. and Cabelguen, J.-M. (1997). Epaxial and limb muscle activity during swimming and terrestrial stepping in the adult newt, *Pleurodeles waltl*. *J. Neurophysiol.* **78**, 638-650.

Earhart, G. M. (2013). Dynamic control of posture across locomotor tasks. *Mov. Disord.* **28**, 1501-1508.

Fetcho, J. R. (1992). The spinal motor system in early vertebrates and some of its evolutionary changes. *Brain Behav. Evol.* **40**, 82-97.

Fish, F. E. (1984). Kinematics of undulatory swimming in the American alligator. *Copeia* **1984**, 839-843.

Fox, H. (1999). Barbels and barbel-like tentacular structures in sub-mammalian vertebrates: a review. *Hydrobiologia* **403**, 153-193.

Hartmann, M. J. Z. (2011). A night in the life of a rat: vibrissal mechanics and tactile exploration. *Ann. N. Y. Acad. Sci.* **1225**, 110-118.

Kajikawa, Y. and Hackett, T. A. (2005). Entropy analysis of neuronal spike train synchrony. *J. Neurosci. Methods* **149**, 90-93.

King, W. M. (2013). Getting ahead of oneself: anticipation and the vestibulo-ocular reflex. *Neuroscience* **236**, 210-219.

Kovac, M. P. and Davis, W. J. (1980). Neural mechanism underlying behavioral choice in *Pleurobranchaea*. *J. Neurophysiol.* **43**, 469-487.

Lambert, F. M., Combes, D., Simmers, J. and Straka, H. (2012). Gaze stabilization by efference copy signaling without sensory feedback during vertebrate locomotion. *Curr. Biol.* **22**, 1649-1658.

Liu, H., Wassersug, R. and Kawachi, K. (1997). The three-dimensional hydrodynamics of tadpole locomotion. *J. Exp. Biol.* **200**, 2807-2819.

Maladen, R. D., Ding, Y., Li, C. and Goldman, D. I. (2009). Undulatory swimming in sand: subsurface locomotion of the sandfish lizard. *Science* **325**, 314-318.

Manter, J. T. (1940). The mechanics of swimming in the alligator. *J. Exp. Zool.* **83**, 345-358.

Maricich, S. M., Wellnitz, S. A., Nelson, A. M., Lesniak, D. R., Gerling, G. J., Lumpkin, E. A. and Zoghbi, H. Y. (2009). Merkel cells are essential for light-touch responses. *Science* **324**, 1580-1582.

Nieuwkoop, P. D. and Faber, J. (1994). *Normal Table of Xenopus laevis (Daudin). A Systematical and Chronological Survey of the Development from the Fertilized Egg till the End of Metamorphosis*. New York: Garland Publishing.

Ovalle, W. K. (1979). Neurite complexes with Merkel cells in larval tentacles of *Xenopus laevis*. *Cell Tissue Res.* **204**, 233-241.

Ovalle, W. K., Shinn, S. L. and Nahirney, P. C. (1998). Ultrastructure of the larval tentacle and its skeletal muscle in *Xenopus laevis*. *Tissue Cell* **30**, 216-225.

Poulet, J. F. A. and Hedwig, B. (2007). New insights into corollary discharges mediated by identified neural pathways. *Trends Neurosci.* **30**, 14-21.

Russell, I. J. and Roberts, B. L. (1974). Active reduction of lateral-line sensitivity in swimming dogfish. *J. Comp. Physiol.* **94**, 7-15.

Saitoh, K., Ménard, A. and Grillner, S. (2007). Tectal control of locomotion, steering, and eye movements in lamprey. *J. Neurophysiol.* **97**, 3093-3108.
Sillar, K. T. and Roberts, A. (1988). A neuronal mechanism for sensory gating during locomotion in a vertebrate. *Nature* **331**, 262-265.
Sommer, M. A. and Wurtz, R. H. (2008). Brain circuits for the internal monitoring of movements. *Annu. Rev. Neurosci.* **31**, 317-338.
Sperry, R. W. (1950). Neural basis of the spontaneous optokinetic response produced by visual inversion. *J. Comp. Physiol. Psychol.* **43**, 482-489.
Straka, H. and Simmers, J. (2012). *Xenopus laevis*: An ideal experimental model for studying the developmental dynamics of neural network assembly and sensory-motor computations. *Dev. Neurobiol.* **72**, 649-663.
Straka, H., Baker, R. and Gilland, E. (2001). Rhombomeric organization of vestibular pathways in larval frogs. *J. Comp. Neurol.* **437**, 42-55.
von Holst, E. and Mittelstaedt, H. (1950). Das Reafferenzprinzip. *Naturwissenschaften* **37**, 464-476.
von Uckermann, G., Le Ray, D., Combes, D., Straka, H. and Simmers, J. (2013). Spinal efference copy signaling and gaze stabilization during locomotion in juvenile *Xenopus* frogs. *J. Neurosci.* **33**, 4253-4264.
Wada, H. (1998). Evolutionary history of free-swimming and sessile lifestyles in urochordates as deduced from 18S rDNA molecular phylogeny. *Mol. Biol. Evol.* **15**, 1189-1194.
Wada, N., Hori, H. and Tokuriki, M. (1993). Electromyographic and kinematic studies of tail movements in dogs during treadmill locomotion. *J. Morphol.* **217**, 105-113.
Wassersug, R. J. and Hoff, K. (1985). The kinematics of swimming in anuran larvae. *J. Exp. Biol.* **119**, 1-30.